

Variation of microphysics in wind bubbles: an alternative mechanism for explaining the rebrightenings in GRB afterglows

S. W. Kong^{1,2}, A. Y. L. Wong², Y. F. Huang¹ and K. S. Cheng^{2*}

¹*Department of Astronomy, Nanjing University, Nanjing 210093, China*

²*Department of Physics, The University of Hong Kong, Pokfulam Road, Hong Kong, China*

Accepted ? December ?. Received ? December ?; in original form ? October ?

ABSTRACT

Conventionally, long GRBs are thought to be caused by the core collapses of massive stars. During the lifetime of a massive star, a stellar wind bubble environment should be produced. Furthermore, the microphysics shock parameters may vary along with the evolution of the fireball. Here we investigate the variation of the microphysics shock parameters under the condition of wind bubble environment, **and allow the microphysics shock parameters to be discontinuous at shocks in the ambient medium. It is found that our model can acceptably reproduce the rebrightenings observed in GRB afterglows, at least in some cases.** The effects of various model parameters on rebrightenings are investigated. The rebrightenings observed in both the R-band and X-ray afterglow light curves of GRB 060206, GRB 070311 and GRB 071010A are reproduced in this model.

Key words: gamma rays: bursts — ISM: jets and outflows — stars: mass loss.

1 INTRODUCTION

Gamma-ray bursts (GRBs) are attractive astrophysics phenomena and had puzzled astronomers for about twenty-four years after their discovery in 1973 (Klebesadel et al. 1973). The discovery of long-lived, multi-band counterparts of GRBs, namely, the afterglows of GRBs, in 1997 is a watershed in GRB research (Costa et al. 1997; Van Paradijs et al. 1997; Frail et al. 1997). Soon after that, the so-called fireball model is recognized as the standard model in view of the fact that it can explain most features of GRB observations well. However, as the advance of observation techniques and the accumulation of observational data, especially after the launch of *Swift* satellite (Gehrels 2004), a lot of unexpected behaviours appear in GRB afterglows, such as the canonical steep-shallow-normal decay and flares in X-ray afterglows, the flattish decay phase and various rebrightenings in optical afterglows (For review, see Zhang 2007).

In fact, there are more and more rebrightenings detected in GRB afterglows, including GRB 970508 (Galama et al. 1998a), GRB 990123 (Sari & Piran 1999), GRB 021004 (Lazzati et al. 2002), GRB 030329 (Berger et al. 2003), GRB 050525A (Blustin et al. 2006), GRB 050820A (Cenko et al. 2006), GRB 050721 (Antonelli et al. 2006), GRB 060206 (Stanek et al. 2007; Liu et al. 2008), GRB 070125 (Up-

dike et al. 2008), GRB 070311 (Guidorzi et al. 2007a), GRB 071003 (Perley et al. 2008), GRB 071010A (Covino et al. 2008). Many different mechanisms have been proposed to explain these rebrightenings, such as density jump (Lazzati et al. 2002; Dai & Wu 2003; Tam et al. 2005), energy injection (Huang et al. 2006), two-component jet (Huang et al. 2004, 2006; Liu et al. 2008), reverse shock (Sari & Piran 1999), reverberation of the energy input measured by prompt emission (Vestrand et al. 2006), turn-on of the external shock (Stanek et al. 2007; Molinari et al. 2007), large angle emission (Panaitescu & Kumar 2007), and spectral peak of existing forward shock (Shao & Dai 2005).

Among all the mechanisms, the density jump model needs to be paid special attention to, because density jump in surrounding medium of GRBs is a very natural hypothesis. Since there are more and more examples indicating that some GRBs are associated with Type Ic supernovae (e.g. SN 1998bw/GRB980425, Galama et al. 1998b; SN2003dh/GRB030329, Price et al. 2003) and many host galaxies of GRBs are in process of active star formation (Fruchter et al. 1999; Djorgovski et al. 1998), it is believed that the progenitors of long GRBs are massive Wolf-Rayet (WR) stars (Woosley 1993). Massive stars usually produce very strong stellar wind to push the initial interstellar medium (ISM) in their neighborhood away during their lifetime. The surrounding of these GRBs should be a wind bubble following the density profile $\rho \propto r^{-2}$ rather

* E-mail: hrspsc@hkucc.hku.hk (KSC)

than the usual homogeneous ISM. Several authors (Castor et al. 1975; Weaver 1977; Ramirez-Riu et al. 2001) further found that beyond some typical radius of the wind bubble, the swept-up mass is too large to be pushed by the wind. As a result, the wind materials pile up at the edge of the wind bubble to form a density jump.

Lazzati et al. (2002) proposed that a density jump can lead to a rebrightening in the afterglow. In usual case, when the observing frequency is between the peak frequency (ν_m) and the cooling frequency (ν_c), the amplitude of the rebrightening should be proportional to the square root of the density contrast. However, if the density contrast is too high, the rebrightening will be weakened, since ν_c will decrease and become less than the observing frequency. In the more detailed numerical simulations by Huang et al. (2007), no obvious rebrightenings can be discriminated when the density jump amplitude is set to 100, which suggests that the simple density jump model is not an ideal mechanism to produce the rebrightenings. In the recent studies by Nakar & Granot (2007) and van Eerten et al. (2009), a full treatment of the transient features at the jump moment, even including the thickness of the blastwave, was considered. Thus these studies should be a more accurate approximation to the reality. Interestingly, no obvious rebrightenings associated with the density jumps are found.

In short, a simple density jump model is difficult to explain the observed rebrightenings in GRB afterglows. On the other hand, the early afterglows of most GRBs exhibit flattish decays with $\alpha < 0.8$, where α is defined as $F_\nu \propto t^{-\alpha}$. This is difficult to explain using the standard fireball model when the density profile is $\rho \propto r^{-2}$. Some previous works have suggested that the microphysics parameters may vary during the evolution of the fireball (Rossi & Rees 2003; Ioka et al. 2006; Fan & Piran 2006; Panaitescu et al. 2006; Granot, Königl & Piran 2006). We believe that this kind of variation could resolve these problems.

In this paper, we show that the observed rebrightenings in GRB afterglows can be well reproduced by assuming varying microphysics shock parameters associated with the wind bubble environments. The outline of our paper is as follows: in §2 we introduce our model detailedly. We then numerically investigate the effects of various parameters on the afterglows in §3, and reproduce the R-band and X-ray afterglow light curves of GRB 060206, GRB 070311 and GRB 071010A in §4. Our discussion and conclusions are presented in §5. We use an assumptive cosmology of $H_0 = 65 \text{ km s}^{-1} \text{ Mpc}^{-1}$, $\Omega_M = 0.30$ and $\Omega_\Lambda = 0.70$ throughout the paper.

2 MODEL

2.1 Dynamics and radiation process

In the standard fireball model, the outflow of GRB, which moves relativistically, interacts with the surrounding medium to form an external shock. A constant fraction ξ_e of the shock energy will be transferred to the swept-up electrons and accelerate them to relativistic velocity. Similarly, a constant fraction ξ_B of the shock energy will go to the magnetic field. These shocked relativistic electrons move in the magnetic field and emit synchrotron radiation to produce broadband afterglows.

We use the convenient equations developed by Huang et al. (1999, 2000a, 2000b, 2003) to describe the dynamics and radiation process of the ejecta. The evolution of the bulk Lorentz factor γ , the shock radius R , and the swept-up medium mass m , is described by three differential equations,

$$\frac{d\gamma}{dm} = -\frac{\gamma^2 - 1}{M_{\text{ej}} + \epsilon m + 2(1 - \epsilon)\gamma m}, \quad (1)$$

$$\frac{dR}{dt} = \beta c \gamma (\gamma + \sqrt{\gamma^2 - 1}), \quad (2)$$

$$\frac{dm}{dR} = 2\pi R^2 (1 - \cos\theta) n m_p, \quad (3)$$

where m_p is proton mass, M_{ej} is the initial mass of the outflow, θ is the half opening angle of the jet, n is the number density of the environment, $\beta = \sqrt{\gamma^2 - 1}/\gamma$, and $\hat{\gamma} \approx (4\gamma + 1)/(3\gamma)$ is the adiabatic index (Dai, Huang, & Lu 1999). ϵ is the radiative efficiency, which equals 1 for a highly radiative case, and equals 0 in the adiabatic case. We ignore the sideways expansion of the jet in our model, because many numerical simulations indicate that it is a very slow process (Granot et al. 2001; Cannizzo, Gehrels & Vishniac 2004; Zhang & MacFadyen 2009). We consider that the afterglow flux mainly comes from the synchrotron radiation of the shocked relativistic electrons.

Since the speed of light (c) is finite, photons received by the observer at a particular time t are not radiated simultaneously, but come from a distorted ellipsoid determined by

$$t = \int \frac{1 - \beta \cos\Theta}{\beta c} dR \equiv \text{const}, \quad (4)$$

within the jet boundaries, where Θ is the angle between the velocity of emitting material and the line of sight. This is the so-called EATS effect. We integrate over the EATS to obtain an accurate observed flux in our simulations (see Huang et al. 2007 for more details).

2.2 Environment

Massive stars usually produce very strong stellar wind during their lifetime. This stellar wind interacts with the initial ISM and forms two shocks: a reverse shock propagates back into the stellar wind and a forward shock that propagates into the ISM. The resulting surrounding medium is broken into four regions (Castor et al. 1975; Weaver 1977; Ramirez-Riu et al. 2005; Pe'er and Wijers 2006) as shown in Figure 1. They are (from inside to outside): (1) the unshocked stellar wind; (2) the shocked stellar wind; (3) the shocked ISM; (4) the unshocked ISM.

Region (1) is a stellar wind bubble. The number density of this region is given by

$$n_1 = \frac{\dot{M}}{4\pi m_p v_w r^2} \propto r^{-2}, \quad (5)$$

where \dot{M} is the mass loss rate of the progenitor, v_w is the launching speed of the stellar wind and r is the radial distance from the central star. We fix v_w as 10^8 cm s^{-1} and only vary \dot{M} in our simulations, since the density profile of the environment only depends on the ratio \dot{M}/v_w .

As the stellar wind expands, the swept-up mass of the ISM increases and is finally comparable to the mass in the

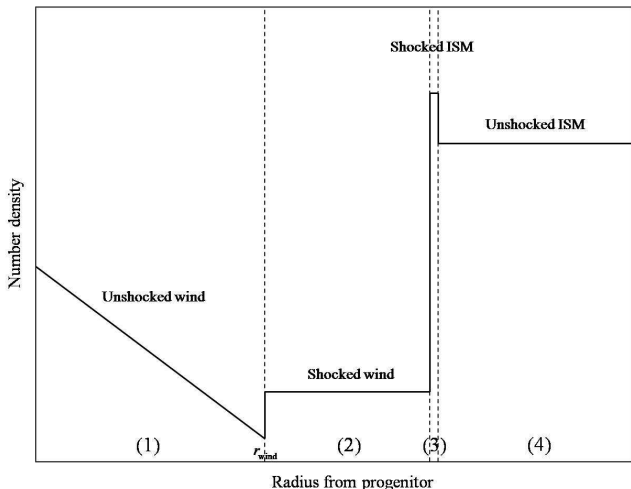


Figure 1. The illustration of the density profile used in our model.

wind at a radius r_{wind} , which is determined by (Ramirez-Ruiz et al. 2001, 2005)

$$r_{\text{wind}} = 1.6 \times 10^{18} \dot{M}_{-6}^{3/10} n_{\text{ISM},3}^{-3/10} v_{w,8}^{1/10} t_{*,6}^{2/5} \text{ cm}, \quad (6)$$

where $n_{\text{ISM},3}$ is the initial density of the homogeneous ISM, in units of 10^3 cm^{-3} , and $t_{*,6}$ is the life time of the WR phase of the star, in units of 10^6 yr . Beyond this radius, in region (2), the swept-up mass is too large to be pushed away by the wind. The material piles up in this region to form a density jump. Because of the effect of the reverse wind shock, the material is hot in this region. The density is approximately constant and equals to $n_2 = 4n_1(r_{\text{wind}})$, where $n_1(r_{\text{wind}})$ is the density in region (1) at the radius of $r = r_{\text{wind}}$.

As shown by Castor et al. (1975), the boundary between Region (2) and Region (3) is at the radius of

$$r_{2-3} = 1.6 \times 10^{19} \dot{M}_{-6}^{1/5} n_{\text{ISM},3}^{-1/5} v_{w,8}^{2/5} t_{*,6}^{3/5} \text{ cm}. \quad (7)$$

Region (3) is a thin, dense shell containing most of the swept-up ISM. Its width is only about $r_{2-3}/12$ and the density in this region is about $4n_{\text{ISM}}$. Here n_{ISM} is also the density in region (4).

We use the density profile introduced above as the environment surrounding GRBs in this paper. As discussed by Pe’er and Wijers (2006), for a GRB event, the blast wave can not reach Region (3) in the relativistic phase. Our numerical results also prove that the fireball is in Region (1) and Region (2) during typical observable time. So we only use Region (1) and Region (2) as the environment in our work. For simplicity, we take r_{wind} as a free parameter in our calculations, so that we do not need to consider the detailed values of v_w and t_* .

Unfortunately, the simple density jump model alone is difficult to explain the rebrightenings in GRB afterglows (Huang et al. 2006, 2007; Nakar & Granot 2007). Moreover, the early optical and/or X-ray afterglow light curves of some GRBs are flatter than the prediction of a normal fireball in a simple wind environment. So we need to consider other effects. Varying microphysics shock parameters should be a possible solution.

2.3 Microphysics parameters

In the standard afterglow model, it is usually assumed that the microphysical parameters are constant throughout the evolution of the fireball. However, the actual microphysical processes in the relativistic shocks, for example, the energy transfer from protons to electrons and magnetic fields, are still not clearly known. It is possible that the microphysical parameters are variational. In fact, the variation of the microphysics parameters during the evolution of the fireball has been considered in many previous studies (Rossi & Rees 2003; Ioka et al. 2006; Fan & Piran 2006; Panaitescu et al. 2006; Granot, Königl & Piran 2006). Fan & Piran (2006) and Panaitescu et al. (2006) have engaged the assumption that the equipartition factors ξ_e and ξ_B are functions of γ to explain the shallow decay phase in some X-ray afterglows. Here we will use a similar idea to investigate the observed rebrightenings in GRB afterglows.

In our model, the circum-burst environment is divided into two parts, i.e. Region (1) and Region (2). The material in Region (1) is the unshocked stellar wind thrown by the mass star. In Region (2) the material consists of the shocked stellar wind mixed with a small fraction of the swept-up ISM. It is hot because of the effect of the reverse wind shock (Castor et al. 1975; Weaver 1977; Ramirez-Ruiz et al. 2005; Pe’er and Wijers 2006). We can imagine that the physical condition, such as the strength of the magnetic field, the temperature and density of the material, could be different between these two regions, so the evolution of microphysics parameters may also be different accordingly. In our study, we use different parameters for these two regions. We assume that

$$\xi_e = \xi_{e,0} \gamma^{-\alpha_1}, \quad (8)$$

$$\xi_B = \xi_{B,0} \gamma^{-\alpha_1} \quad (9)$$

in Region (1), and

$$\xi_e = \xi_{e,0} \gamma^{-\alpha_2}, \quad (10)$$

$$\xi_B = \xi_{B,0} \gamma^{-\alpha_2} \quad (11)$$

in Region (2).

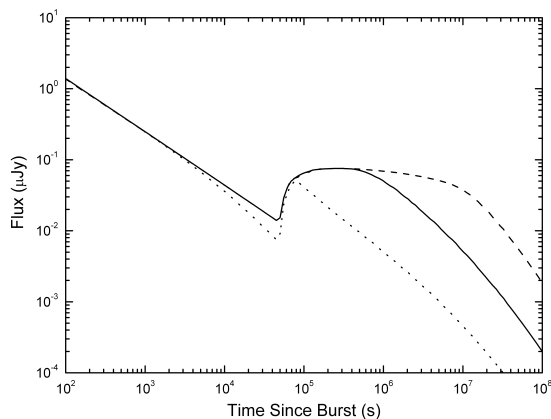
3 NUMERICAL RESULTS

In this section, we present our numerical results to show the effects of various physical parameters on the R-band light curves, using the model described in §2. For convenience, we first define a set of “standard” parameters, as shown in the second column of Table 1.

Figure 2 illustrates the effect of the parameter θ_0 on the R-band light curves. The solid line corresponds to the “standard” parameters. The dashed line corresponds to $\theta_0 = 0.3$ rad and the dotted line corresponds to $\theta_0 = 0.03$ rad. We can see that when the change of microphysics parameters is considered, an obvious rebrightening appears. Interestingly, when θ_0 is larger, the duration of the rebrightening becomes longer. This is not difficult to understand. The afterglow brightness is dominated by the high latitude emission, so that the EATS shows a ring-like pattern. As a result, the brightness will be kept on a relatively higher level after the

Table 1. Modeling Parameters

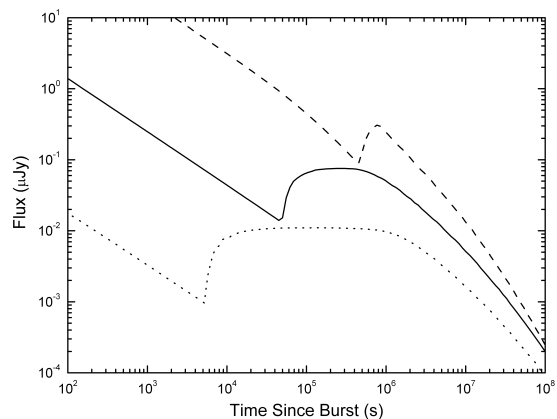
| Parameters | Standard | GRB 060206 | GRB 070311 | GRB 071010A |
|-----------------------------------|----------------------|----------------------|----------------------|----------------------|
| z | 1.0 | 4.045 | 1.0 | 0.98 |
| E_0 (ergs) | 1.0×10^{53} | 9.0×10^{52} | 8.0×10^{51} | 1.3×10^{52} |
| θ_0 (rad) | 0.1 | 0.06 | 0.08 | 0.11 |
| \dot{M} (M_\odot/yr) | 1.0×10^{-6} | 2.0×10^{-5} | 6.0×10^{-6} | 4.0×10^{-5} |
| r_{wind} (cm) | 1.0×10^{18} | 3.0×10^{16} | 2.0×10^{17} | 5.1×10^{16} |
| p | 2.5 | 2.2 | 2.3 | 2.1 |
| $\xi_{e,0}$ | 0.1 | 0.3 | 0.3 | 0.3 |
| $\xi_{B,0}$ | 0.01 | 0.03 | 0.03 | 0.03 |
| $\alpha 1$ | 1.5 | 1.2 | 0.9 | 1.5 |
| $\alpha 2$ | 1.3 | 0.6 | 0.0 | 0.6 |

**Figure 2.** The effect of the parameter θ_0 on the R-band light curve. The solid line corresponds to the standard parameters. The dashed line corresponds to $\theta_0 = 0.3$ rad and the dotted line corresponds to $\theta_0 = 0.03$ rad.

density jump moment, to form a flat phase. When θ_0 becomes larger, the time delay of the photons from the edge of the outflow also becomes larger. So the flat phase is longer.

Environment is an important factor that affects the evolution of GRB afterglows. As mentioned before, the character of wind environment is mainly determined by the ratio \dot{M}/v_w . We fix v_w as 10^8 cm s $^{-1}$ and only vary \dot{M} here to investigate the effect of the parameter \dot{M} on the R-band light curves. The results are shown in Figure 3. The solid line corresponds to the “standard” parameters. The dashed line corresponds to $\dot{M} = 1.0 \times 10^{-5} M_\odot/\text{yr}$ and the dotted line corresponds to $\dot{M} = 1.0 \times 10^{-7} M_\odot/\text{yr}$. It is clearly seen that for a smaller \dot{M} value, the rebrightening appears earlier and the flux before the rebrightening are lower. This result is easy to understand. A smaller \dot{M} corresponds to a smaller density, and the deceleration of the external shock is slower. So the Lorentz factor is larger and the fireball can meet the density jump earlier. A larger Lorentz factor also makes ξ_e and ξ_B smaller and decreases the flux.

The parameter r_{wind} is another factor to describe the character of the environment. The effect of r_{wind} on the R-band light curve is illustrated in Figure 4. The solid line corresponds to the “standard” parameters. The dashed line

**Figure 3.** The effect of the parameter \dot{M} on the R-band light curve. The solid line corresponds to the “standard” parameters. The dashed line corresponds to $\dot{M} = 1.0 \times 10^{-5} M_\odot/\text{yr}$ and the dotted line corresponds to $\dot{M} = 1.0 \times 10^{-7} M_\odot/\text{yr}$.

corresponds to $r_{\text{wind}} = 5.0 \times 10^{18}$ cm and the dotted line corresponds to $r_{\text{wind}} = 5.0 \times 10^{17}$ cm. We can see that the rebrightening appears earlier when r_{wind} is smaller, because r_{wind} determines the position of the density jump.

The effect of the parameter $\alpha 1$ on the R-band light curve is shown in Figure 5. The solid line corresponds to the “standard” parameters. The dashed line corresponds to $\alpha 1 = 1.7$ and the dotted line corresponds to $\alpha 1 = 1.3$. It is obvious that a larger $\alpha 1$ makes the flux before the rebrightening lower. This is not difficult to understand. With the increase of $\alpha 1$, the values of ξ_e and ξ_B before the rebrightening become smaller. This suppresses the radiation flux at early time.

The effect of the parameter $\alpha 2$ on the R-band light curve is illustrated in Figure 6. The solid line corresponds to the “standard” parameters. The dashed line corresponds to $\alpha 2 = 1.5$ and the dotted line corresponds to $\alpha 2 = 1.1$. As expected, the effect of $\alpha 2$ is similar to that of $\alpha 1$ for the same reason.

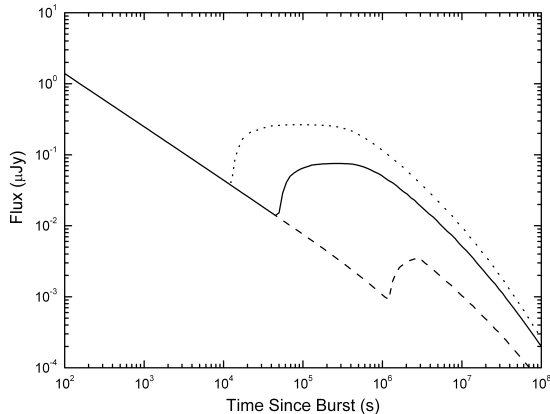


Figure 4. The effect of the parameter r_{wind} on the R-band light curve. The solid line corresponds to the “standard” parameters. The dashed line corresponds to $r_{\text{wind}} = 5.0 \times 10^{18}$ cm and the dotted line corresponds to $r_{\text{wind}} = 50 \times 10^{17}$ cm.

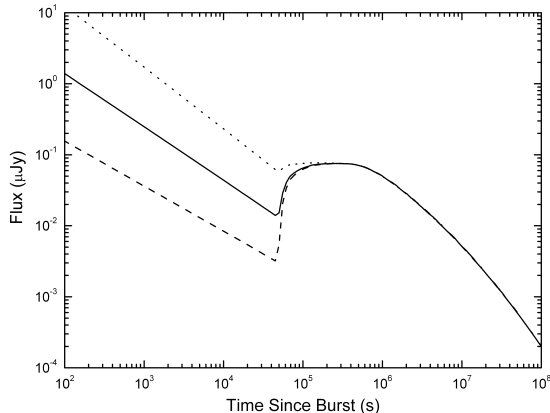


Figure 5. The effect of the parameter α_1 on the R-band light curve. The solid line corresponds to the “standard” parameters. The dashed line corresponds to $\alpha_1 = 1.7$ and the dotted line corresponds to $\alpha_1 = 1.3$.

4 COMPARISON WITH OBSERVATIONS

In this section we select three GRBs with obvious rebrightenings in both optical and X-ray bands, i.e. GRB 060206, GRB 070311 and GRB 071010A, and reproduce their R-band and X-ray afterglow light curves numerically, using the model described in §2.

4.1 GRB 060206

GRB 060206 was detected at 04:46:53 UT on Feb. 6 by the Burst Alert Telescope (BAT) onboard the *Swift* satellite (Morris et al. 2006). The temporal profile of the BAT light curve shows a single peak, with a total fluence of $8.4 \pm 0.4 \times 10^{-7}$ erg cm $^{-2}$ in the 15-350 keV band (Mor-

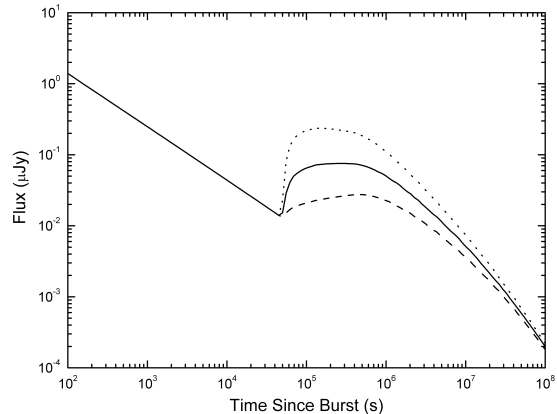


Figure 6. The effect of the parameter α_2 on the R-band light curve. The solid line corresponds to the “standard” parameters. The dashed line corresponds to $\alpha_2 = 1.5$ and the dotted line corresponds to $\alpha_2 = 1.1$.

ris et al. 2006; Palmer et al. 2006). The total duration of the burst is $T_{90} = 7 \pm 2$ s, suggesting that it is a long-duration GRB (Palmer et al. 2006).

The UVOT telescope onboard the *Swift* satellite first observed the optical afterglow of GRB 060206 and found it located at the position of $\alpha = 13^{\text{h}}31^{\text{m}}43^{\text{s}}.416$, $\delta = +35^{\circ}03'03''.6$ (J2000.0; Boyd et al. 2006), corresponding to the Galactic extinction of $A_R = 0.033$ mag (Schlegel, Finkbeiner & Davis 1998). After that, a number of telescopes made detailed follow up observations, such as the 2-m robotic Liverpool Telescope (Monfardini et al. 2006), the Rapid Telescopes for Optical Response (RAPTOR; Woźniak et al. 2006) and the MDM telescope (Stanek et al. 2007). From the calibrated ALFOSC spectrum of the afterglow, Fynbo et al. (2006) determined the redshift of GRB 060206 as $z = 4.045$. X-ray afterglow was also detected by XRT on *Swift* at 58 s after the trigger (Morris et al. 2006).

There are significant rebrightenings in both the optical and X-ray afterglows of GRB 060206 at about 3000 s after the burst. Liu et al. (2008) suggested that the rebrightening comes from a jet-like ejecta with a larger viewing angle, which is produced by the central engine.

Here we try to use our model described in §2 to reproduce the rebrightenings in both R-band and X-ray light curves of GRB 060206. Our best-fit physical parameters are presented in Table 1, and our modeling curves are illustrated in Figure 7. The observed R-band data are taken from Monfardini et al. (2006), Woźniak et al. 2006 and Stanek et al. (2007), and the X-ray data are taken from the *Swift* XRT light curve repository¹ (Evans et al. 2007). We can see in Figure 7 that our model can generally reproduce the light curves well. Note that at the late stage, the observed X-ray light curve is obviously too flat as compared with our theoretical result. This may be due to the contamination from a nearby source, as already mentioned by Stanek et al. (2007).

¹ http://www.swift.ac.uk/xrt_curves/

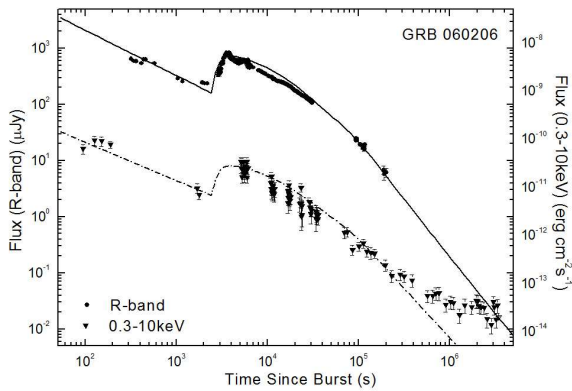


Figure 7. Our best fit to the R-band and X-ray afterglow light curves of GRB 060206. The lines are our theoretical curves and the fitting parameter values are given in Table 1. The R-band observed data are taken from Monfardini et al. (2006), (Woźniak et al. 2006) and Stanek et al. (2007), and the X-ray data are taken from the *Swift* XRT light curve repository (Evans et al. 2007). All optical data points have been corrected for the Galactic extinction (Schlegel, Finkbeiner & Davis 1998).

4.2 GRB 070311

GRB 070311 occurred at 01:52:50 UT on 2007 March 11 and was detected by the INTEGRAL/IBAS in IBIS/ISGRI data. The duration of the γ -ray prompt emission is about 50 s in the 20-200 keV band, with the peak flux of $0.9 \text{ photons cm}^{-2} \text{ s}^{-1}$ (1 s integration time) and the total fluence of $2 \times 10^{-6} \text{ erg cm}^{-2}$ (Mereghetti et al. 2007).

The afterglow of GRB 070311 was first discovered by the Rapid Eye Mount (REM) telescope at 55 s after the burst. A bright fading source was found at $\alpha = 05^{\text{h}}50^{\text{m}}08^{\text{s}}.21$, $\delta = +03^{\circ}22'30''.3$ (J2000.0; Covino et al. 2007). This location has a low Galactic latitude ($l = 202^{\circ}.766$, $b = -11^{\circ}.998$ in Galactic coordinates), so the Galactic extinction is as much as $A_R = 2.038 \text{ mag}$ (Schlegel, Finkbeiner & Davis 1998). X-ray afterglow was also found by the observations of XRT on *Swift* at about 7000 s after the trigger (Guidorzi et al., 2007b).

The optical afterglow of GRB 070311 has complex structures. Besides a normal power law decay, there are two fast rise exponential decay (FRED) shaped pulses peaking around 80 and 140 s after the peak of the GRB and possibly accompanied by the tail of prompt γ -ray emission (Guidorzi et al. 2007a). Another structure, which is the most attractive feature, is a significant late rebrightening between 3×10^4 s and 2×10^5 s after the trigger in both optical and X-ray bands (Guidorzi et al. 2007a). Guidorzi et al. (2007a) have used a power law function plus a FRED shaped pulse to fit the afterglows in both R and X-ray bands. More physically, they suggested that the late afterglow rebrightening of GRB 070311 can come from a refreshed shock. Additionally, they argued that the density jump in the surrounding medium can be the origin of the rebrightening too, but less appealing.

Here we use our model described in §2 to reproduce the late rebrightenings in both R-band and X-ray light curves

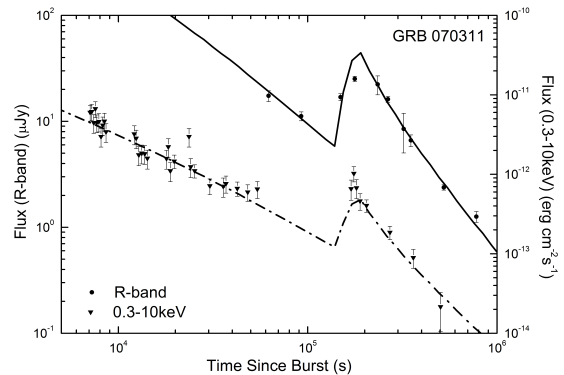


Figure 8. Our best fit to the late rebrightenings in the R-band and X-ray light curves of GRB 070311. The lines are our theoretical curves and the fitting parameter values are given in Table 1. The R-band observed data are taken from Guidorzi et al. (2007a; for REM data) and GCN circulars (Cenko 2007; Dai et al. 2007; Garnavich et al. 2007; Halpern & Armstrong 2007a,b,c,d; Jelínek, Kubánek & Prouza 2007; Kann 2007; Wren et al. 2007), and the X-ray data are taken from the *Swift* XRT light curve repository (Evans et al. 2007). All optical data points have been corrected for the Galactic extinction (Schlegel, Finkbeiner & Davis 1998).

of GRB 070311. We take the observed R-band data from Guidorzi et al. (2007a; for REM data) and GCN circulars (Cenko 2007; Dai et al. 2007; Garnavich et al. 2007; Halpern & Armstrong 2007a,b,c,d; Jelínek, Kubánek & Prouza 2007; Kann 2007; Wren et al. 2007), and the X-ray data from the *Swift* XRT light curve repository (Evans et al. 2007). Because the redshift of GRB 070311 is still unknown, we simply assume a redshift of $z = 1.0$ in our calculation. Our best-fit physical parameters are presented in Table 1, and our modeling curves are illustrated in Figure 8. We see that the interpretation of our model to this event is also generally acceptable.

4.3 GRB 071010A

GRB 071010A triggered the *Swift* satellite at 03:41:12 UT on 2007 Oct. 10 (Moretti et al. 2007). It is a traditional long GRB with the burst duration of $T_{90} = 6 \pm 1 \text{ s}$. The total fluence of the burst is about $2.0 \times 10^{-7} \text{ erg cm}^{-2}$ (Krimm et al. 2007).

TAROT telescope identified the optical afterglow of GRB 071010A firstly, only 124 s after the trigger (Klotz, Boer & Atteia, 2007). Bloom et al. (2007) further found that the position of the burst was $\alpha = 19^{\text{h}}12^{\text{m}}14^{\text{s}}.624$, $\delta = -32^{\circ}24'07''.16$ (J2000.0), corresponding to the Galactic extinction of $A_R = 0.263 \text{ mag}$ (Schlegel, Finkbeiner & Davis 1998). Spectral observations were done subsequently by Keck and the analysis of the Mg II and Fe II lines gave the redshift of the burst as $z = 0.98$ (Prochaska et al. 2007). X-ray data were also acquired by XRT observations on *Swift* (Guidorzi et al. 2007b), but no radio afterglow was detected at 8.46 GHz until almost 2 days after the burst (Chandra & Frail 2007).

The most interesting feature of the afterglows of GRB 071010A is the appearance of a sharp rebrightening at about

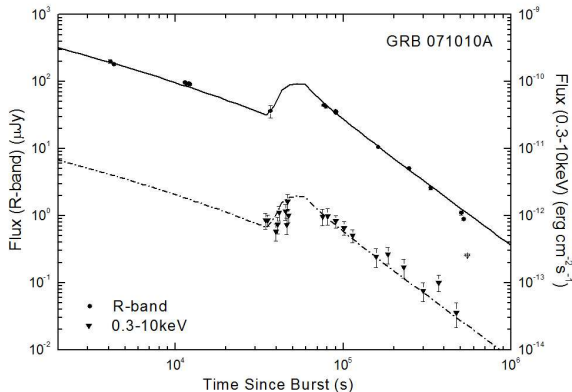


Figure 9. Our best fit to the R-band and X-ray afterglow light curves of GRB 071010A. The lines are our theoretical curves and the fitting parameter values are given in Table 1. The R-band observed data are taken from Covino et al. (2008), and the X-ray data are taken from the *Swift* XRT light curve repository (Evans et al. 2007). All data points have been corrected for the Galactic extinction (Schlegel, Finkbeiner & Davis 1998).

0.6 days after the GRB, clearly seen in both optical and X-ray bands. Covino et al. (2008) have used a Beuermann et al. (1999) function, and a simple step function for the rebrightening, to fit the afterglows. They suggested that the rebrightening was due to an injection of abundant energy, which was comparable to the initial energy in the fireball. The steepening after the rebrightening was interpreted as a jet break at around 1 day after the burst.

We try to use our model introduced in §2 to reproduce the R-band and X-ray light curves of GRB 071010A. In our modeling, the observed R-band data are taken from Covino et al. (2008), and the X-ray data are taken from the *Swift* XRT light curve repository (Evans et al. 2007). Our best-fitting physical parameters are presented in Table 1, and our modeling curves are illustrated in Figure 9. It is clear that our model can reproduce the rebrightening features of GRB 071010A very well.

5 DISCUSSION AND CONCLUSION

In the standard fireball model, it is assumed that the circum-burst medium density is constant or following a single $\rho \propto r^{-2}$ law. The microphysics shock parameters are also usually assumed invariable during the evolution of the fireball. These models can basically explain many pre-*Swift* GRB afterglows, whose spectrum and light curves can be approximated as broken power-law functions (Panaitescu & Kumar 2001a, 2001b; Yost et al. 2003). The launch of *Swift* satellite (Gehrels 2004) makes it possible to observe early afterglows of many GRBs in the first few hours after the trigger. Many remarkable and unexpected features are found, such as marked rebrightenings and the flattish decay phase in early GRB afterglows.

In fact, the standard fireball model is obviously too simplified. If long GRBs indeed originate from the death of massive stars, the environment of GRBs should have complex

structures rather than have a constant or single power law profile. Some analytical (Castor et al. 1975; Weaver 1977; Ramirez-Riu et al. 2005; Pe’er and Wijers 2006) and numerical (Ramirez-Riu et al. 2001) studies suggest that the circum-burst density profile should be a wind bubble, associated with a few density jumps. On the other hand, the microphysics parameters, such as ξ_e and ξ_B , may vary during the evolution of the fireball (Rossi & Rees 2003; Ioka et al. 2006; Fan & Piran 2006; Panaitescu et al. 2006; Granot, Königl & Piran 2006). Actually, the fast decrease of the cooling frequency ν_c in some GRBs suggests that ξ_B may be evolving (Panaitescu et al. 2006). Some previous studies also suggest that ξ_e and ξ_B may be different for the forward shock and the reverse shock (Fan et al. 2002; Wei, Yan & Fan 2006), and may also be different for Region (1) and Region (2) (Gebdre et al. 2007; Kamble, Resmi & Misra 2007). So, ξ_e and ξ_B may depend on the strength of the shock and the environment.

In our study, we combine the wind bubble environments and the change of microphysics shock parameters together. Comparing with the standard fireball model, our model has three more parameters (i.e. r_{wind} , $\alpha 1$ and $\alpha 2$). We find that this model can produce the observed rebrightenings and flattish decay in GRB afterglows successfully. We have shown that the observed rebrightenings in both the optical and X-ray afterglow light curves of GRB 060206, GRB 070311 and GRB 071010A can be well explained by our model.

We have also investigated the effects of various parameters on the light curves numerically. We can imagine that if the stellar wind produced by the progenitor is very strong, or the launching speed of the stellar wind v_w is small, or the value of r_{wind} is large enough, there will be no rebrightening within the usual observation time. So, basically the wind bubble environment can also give birth to a steadily decaying afterglow that shows no rebrightening.

In our work, we neglect the effect of the reverse shock. According to the study by Dai & Lu (2002), when an ultra-relativistic blast wave interacts with a density jump medium, the resulting reverse shock is relativistic only if the amplitude of the density jump is much larger than 21. In our model, the amplitude of the density jump is only 4, so the corresponding reverse shock is Newtonian. The emission from the Newtonian reverse shock is very weak, and can be omitted. Moreover, although we use an abrupt density jump, the actual increase of density may be gradual. In this situation, the emission from the reverse shock will even be much weaker.

Currently, a complete understanding of the microphysical processes in the relativistic shocks is still lacking. Using the derived microphysical parameters from GRB modeling, people may be able to get some constraints on the shock physics. The derived parameter values of \dot{M} and m_{ISM} are also very important. They are closely related to the evolution and the environment of the massive star. They may give some hints on the characters of the progenitor, such as the initial main-sequence mass and the metallicity. So, from the modeling parameters, we can also obtain some useful information about GRB origin.

ACKNOWLEDGMENTS

We thank the anonymous referee for stimulating suggestions that lead to an overall improvement of this study. We also would like to thank Kinwah Wu, Z. G. Dai and X. Y. Wang for helpful suggestions and discussion. This research was supported by a 2009 GRF grant of Hong Kong Government (grants 701109), the National Natural Science Foundation of China (grants 10625313), and the National Basic Research Program of China (973 Program 2009CB824800).

REFERENCES

- Antonelli L. A., et al., 2006, *A&A*, 456, 509
 Berger E., et al., 2003, *Nature*, 426, 154
 Beuermann K., et al., 1999, *A&A*, 352, L26
 Bloom J. S., et al., 2007, *GCN Circ.* 6861 (<http://gcn.gsfc.nasa.gov/gcn/gcn3/6861.gcn3>)
 Blustin A. J., et al., 2006, *ApJ*, 637, 901
 Boyd P., Hunsberger S., Gronwall C., 2006, *GCN Circ.* 4684 (<http://gcn.gsfc.nasa.gov/gcn/gcn3/4684.gcn3>)
 Cannizzo J. K., Gehrels N., Vishniac E. T., 2004, *ApJ*, 601, 380
 Castor J., McCray R., Weaver R., 1975, *ApJL*, 200, L107
 Cenko S. B., et al., 2006, *ApJ*, 652, 490
 Cenko S. B., 2007, *GCN Circ.* 6196 (<http://gcn.gsfc.nasa.gov/gcn/gcn3/6196.gcn3>)
 Chandra P., Frail D. A., 2007, *GCN Circ.* 6901 (<http://gcn.gsfc.nasa.gov/gcn/gcn3/6901.gcn3>)
 Costa E., et al., 1997, *Nature*, 387, 783
 Covino S., et al., 2007, *GCN Circ.* 6190 (<http://gcn.gsfc.nasa.gov/gcn/gcn3/6190.gcn3>)
 Covino S., et al., 2008, *MNRAS*, in press ([astro-ph/0804.4367](http://arxiv.org/abs/0804.4367))
 Dai X., et al., 2007, *GCN Circ.* 6219 (<http://gcn.gsfc.nasa.gov/gcn/gcn3/6219.gcn3>)
 Dai Z. G., Huang Y. F., Lu T., 1999, *ApJ*, 520, 634
 Dai Z. G., Lu T., 2002, *ApJL*, 565, L87
 Dai Z. G., Wu X. F., 2003, *ApJL*, 591, L21
 Djorgovski S. G., et al., 1998, *ApJL*, 508, L17
 Evans P. A., et al., 2007, *A&A*, 469, 379
 Fan Y. Z., Dai Z. G., Huang Y. F., Lu T., 2002, *Chin. J. Astron. Astrophys.*, 2, 449
 Fan Y. Z., Piran T., 2006, *MNRAS*, 369, 197
 Frail D. A., et al., 1997, *Nature*, 389, 261
 Fruchter A. S., et al., 1999, *ApJ*, 516, 683
 Fynbo J. P. U., et al., 2006, *GCN Circ.* 4692 (<http://gcn.gsfc.nasa.gov/gcn/gcn3/4692.gcn3>)
 Galama T. J., et al., 1998a, *ApJL*, 497, L13
 Galama T. J., et al., 1998b, *Nature*, 395, 670
 Garnavich P., et al., 2007, *GCN Circ.* 6245 (<http://gcn.gsfc.nasa.gov/gcn/gcn3/6245.gcn3>)
 Gehrels N., et al., 2004, *ApJ*, 611, 1005
 Gebdre B., Galli A., Corsi A., et al., 2007, *A&A*, 462, 565
 Granot J., Königl A., Piran T., 2006, *MNRAS*, 370, 1946
 Granot J., Miller M., Piran T., et al., 2001, in *Gamma-ray Bursts in the Afterglow Era*, Berlin: Springer-Verlag, ed. E. Costa, F. Frontera & J. Hjorth, 312
 Guidorzi C., et al., 2007a, *A&A*, 474, 793
 Guidorzi C., et al., 2007b, *GCN Circ.* 6192 (<http://gcn.gsfc.nasa.gov/gcn/gcn3/6192.gcn3>)
 Guidorzi C., et al., 2007b, *GCN Circ.* 6870 (<http://gcn.gsfc.nasa.gov/gcn/gcn3/6870.gcn3>)
 Halpern J. P., Armstrong E., 2007a, *GCN Circ.* 6195 (<http://gcn.gsfc.nasa.gov/gcn/gcn3/6195.gcn3>)
 Halpern J. P., Armstrong E., 2007b, *GCN Circ.* 6199 (<http://gcn.gsfc.nasa.gov/gcn/gcn3/6199.gcn3>)
 Halpern J. P., Armstrong E., 2007c, *GCN Circ.* 6203 (<http://gcn.gsfc.nasa.gov/gcn/gcn3/6203.gcn3>)
 Halpern J. P., Armstrong E., 2007d, *GCN Circ.* 6208 (<http://gcn.gsfc.nasa.gov/gcn/gcn3/6208.gcn3>)
 Huang Y. F., Cheng K. S., 2003, *MNRAS*, 341, 263
 Huang Y. F., Cheng K. S., Gao, T. T., 2006, *ApJ*, 637, 873
 Huang Y. F., Dai Z. G., Lu T., 1999, *MNRAS*, 309, 513
 Huang Y. F., Dai Z. G., Lu T., 2000a, *MNRAS*, 316, 943
 Huang Y. F., Gou L. J., Dai Z. G., Lu T., 2000b, *ApJ*, 543, 90
 Huang Y. F., Lu Y., Wong A. Y. L., Cheng K. S., 2007, *Chinese J. Astron. Astrophys.*, 7, 397
 Huang Y. F., Wu X. F., Dai Z. G., Ma H. T., Lu T., 2004, *ApJ*, 605, 300
 Ioka K., Toma K., Yamazaki R., Nakamura N., 2006, *A&A*, 458, 7
 Jelínek M., Kubánek P., Prouza M., 2007, *GCN Circ.* 6197 (<http://gcn.gsfc.nasa.gov/gcn/gcn3/6197.gcn3>)
 Kamble A., Resmi L., Misra K., 2007, *ApJL*, 664, L5
 Kann D. A., 2007, *GCN Circ.* 6209 (<http://gcn.gsfc.nasa.gov/gcn/gcn3/6209.gcn3>)
 Klebesadel R. W., Strong I. B., Olson R. A., 1973, *ApJL*, 182, L85
 Klotz A., Boer M., Atteia J.L., 2007, *GCN Circ.* 6860 (<http://gcn.gsfc.nasa.gov/gcn/gcn3/6860.gcn3>)
 Krimm H., et al., 2007, *GCN Circ.* 6868 (<http://gcn.gsfc.nasa.gov/gcn/gcn3/6868.gcn3>)
 Lazzati D., et al., 2002, *A&A*, 396, L5
 Liu X. W., Wu X. F., Lu, T., 2008, *A&A*, 487, 503
 Mereghetti S., et al., 2007, *GCN Circ.* 6189 (<http://gcn.gsfc.nasa.gov/gcn/gcn3/6189.gcn3>)
 Molinari E., et al., 2007, *A&A*, 469, L13
 Monfardini A., et al., 2006, *ApJ*, 648, 1125
 Moretti A., et al., 2007, *GCN Circ.* 6859 (<http://gcn.gsfc.nasa.gov/gcn/gcn3/6859.gcn3>)
 Morris D. C., et al., 2006, *GCN Circ.* 4682 (<http://gcn.gsfc.nasa.gov/gcn/gcn3/4682.gcn3>)
 Nakar E., Granot J., 2007, *MNRAS*, 380, 1744
 Palmer D., et al., 2006, *GCN Circ.* 4697 (<http://gcn.gsfc.nasa.gov/gcn/gcn3/4697.gcn3>)
 Panaitescu A., et al., 2006, *MNRAS*, 369, 2059
 Panaitescu A., Kumar P., 2001a, *ApJ*, 554, 667
 Panaitescu A., Kumar P., 2001b, *ApJL*, 560, L49
 Panaitescu A., Kumar P., 2007, *MNRAS*, 376, 1065
 Pe'er A., Wijers R. A. M. J., 2006, *ApJ*, 643, 1036
 Perley D. A., et al., 2008, *ApJ*, submitted ([astro-ph/0805.2394](http://arxiv.org/abs/0805.2394))
 Price P. A., et al., 2003, *Nature*, 423, 844
 Prochaska J. X., et al., 2007, *GCN Circ.* 6864 (<http://gcn.gsfc.nasa.gov/gcn/gcn3/6864.gcn3>)
 Ramirez-Ruiz E., Dray L. M., Madau P., Tout C. A., 2001, *MNRAS*, 327, 829
 Ramirez-Ruiz E., Carcía-Segura G., Salmonson J. D., Pérez-Rendón B., 2005, *ApJ*, 631, 435
 Rossi E., Rees M. J., 2003, *MNRAS*, 339, 881
 Sari R., Piran T., 1999, *ApJL*, 517, L109

- Schlegel D. J., Finkbeiner D. P., Davis M., 1998, ApJ, 500, 525
- Shao L., Dai Z. G., 2005, ApJ, 633, 1027
- Stanek K. Z., et al., 2007, ApJL, 654, L21
- Tam P. H., Pun C. S. J., Huang Y. F., Cheng K. S., 2005, New Astronomy, 10, 535
- Updike A. C., et al., 2008, ApJ, in press (arXiv:0805.1094)
- van Eerten H. J., Meliani Z., Wijers R. A. M. J., Keppens R., 2009, MNRAS, accepted (arXiv:0906.3629)
- Van Paradijs J., et al., 1997, Nature, 386, 686
- Vestrand W. T., et al., 2006, Nature, 442, 172
- Weaver R., McCray R., Castor J., Shapiro P., Moore M., 1977, ApJ, 218, 377
- Wei D. M., Yan T., Fan Y. Z., 2006, ApJL, 636, L29
- Woosley S. E., 1993, ApJ, 405, 273
- Woźniak P. R., et al., 2006, ApJL, 642 L99
- Wren J., et al., 2007, GCN Circ. 6198 (<http://gcn.gsfc.nasa.gov/gcn/gcn3/6198.gcn3>)
- Yost S. A., Harrison F. A., Sari R., Frail D. A., 2003, ApJ, 597, 459
- Zhang B., 2007, Chinese J. Astron. Astrophys., 7, 1
- Zhang W. Q., MacFadyen A., 2009, ApJ, 698, 1261